ADVANCED ELECTRONIC MATERIALS
www.advelectronicmat.de

Single-Molecule Bioelectronic Label-Free Assay of both Protein and Genomic Markers of Pancreatic Mucinous Cysts' in Whole Blood Serum

Eleonora Macchia, Lucia Sarcina, Caroline Driescher, Zahra Gounani, Amit Tewari, Ronald Osterbacka, Gerardo Palazzo, Angelo Tricase, Zsolt Miklos Kovacs Vajna, Fabrizio Viola, Francesco Modena, Mario Caironi, Fabrizio Torricelli, Irene Esposito, and Luisa Torsi**

The timely diagnosis of cystic pancreatic cancer precursors is of utmost importance to improve patients' low survival rate. Fine-needle aspiration cytology is endowed with low diagnostic sensitivity, while more effective is the assay of markers, such as a mutated *KRAS*, in the cyst fluids. Next-generation sequencing, detecting down to a single copy of a genomic marker, enables early diagnosis but the diagnostic sensitivity of high-grade cysts, likely to become malignant, is low. Assaying both mutated *KRAS* and MUC1 protein markers can improve diagnostic accuracy. Their detection in blood would also be minimally invasive. Here, the mucinous lesions markers, *KRAS* and MUC1, are both successfully assayed in blood serum at the physical limit with the label-free "Single-Molecule assay with a large Transistor—SiMoT." This is a compelling proof of principle that the SiMoT platform holds high potential to enable a timely, minimally invasive, and accurate diagnosis of pancreatic cancer precursor cysts.

1. Introduction

The global incidence of pancreatic cancer increased in the years 1990–2017 from 5.0 to 5.7 per 100 000 person-years, while the number of deaths went up from 196 000 to 441 000.[1] This makes pancreatic cancer the solid tumor with the highest mortality-to-incidence ratio being the 4th cause of cancer-related death in Europe[2] and the 9th cause of death globally,[3,4] with less than 10% of patients surviving for five years.[5] Due to its relatively low overall prevalence, screening of a large population against pancreatic cancer is not recommended. Much more effective is to tackle high-risk groups such as individuals with a genetic predisposition, patients with new-onset diabetes and those with mucinous pancreatic cystic lesions.

Dr. E. Macchia, Dr. Z. Gounani, Dr. A. Tewari, Prof. R. Österbacka, Prof. L. Torsi
Faculty of Science and Engineering
Åbo Akademi University
Turku 20500, Finland
E-mail: luisa.torsi@uniba.it

L. Sarcina, Prof. G. Palazzo, A. Tricase, Prof. L. Torsi
Dipartimento di Chimica
Università degli Studi di Bari "Aldo Moro"
Bari 70125, Italy

C. Driescher, Prof. I. Esposito
Institute of Pathology
Heinrich-Heine University and University Hospital of Düsseldorf
Duesseldorf 40225, Germany
E-mail: irene.esposito@med.uni-duesseldorf.de

The ORCID identification number(s) for the author(s) of this article can be found under https://doi.org/10.1002/aelm.202100304.

DOI: 10.1002/aelm.202100304

Prof. G. Palazzo, Prof. L. Torsi
Centre for Colloid and Surface Science–Università degli Studi di Bari "Aldo Moro"
Bari 70125, Italy

Prof. Z. M. Kovacs Vajna, Prof. F. Torricelli
Dipartimento Ingegneria dell'Informazione
Università degli Studi di Brescia
Brescia 25123, Italy

Dr. F. Viola, F. Modena, Dr. M. Caironi
Center for Nano Science and Technology@PoliMi
Istituto Italiano di Tecnologia
Milan 20133, Italy

F. Modena
Dipartimento di Elettronica
Infomazione e Bioingegneria
Politecnico di Milano
Milano 20133, Italy

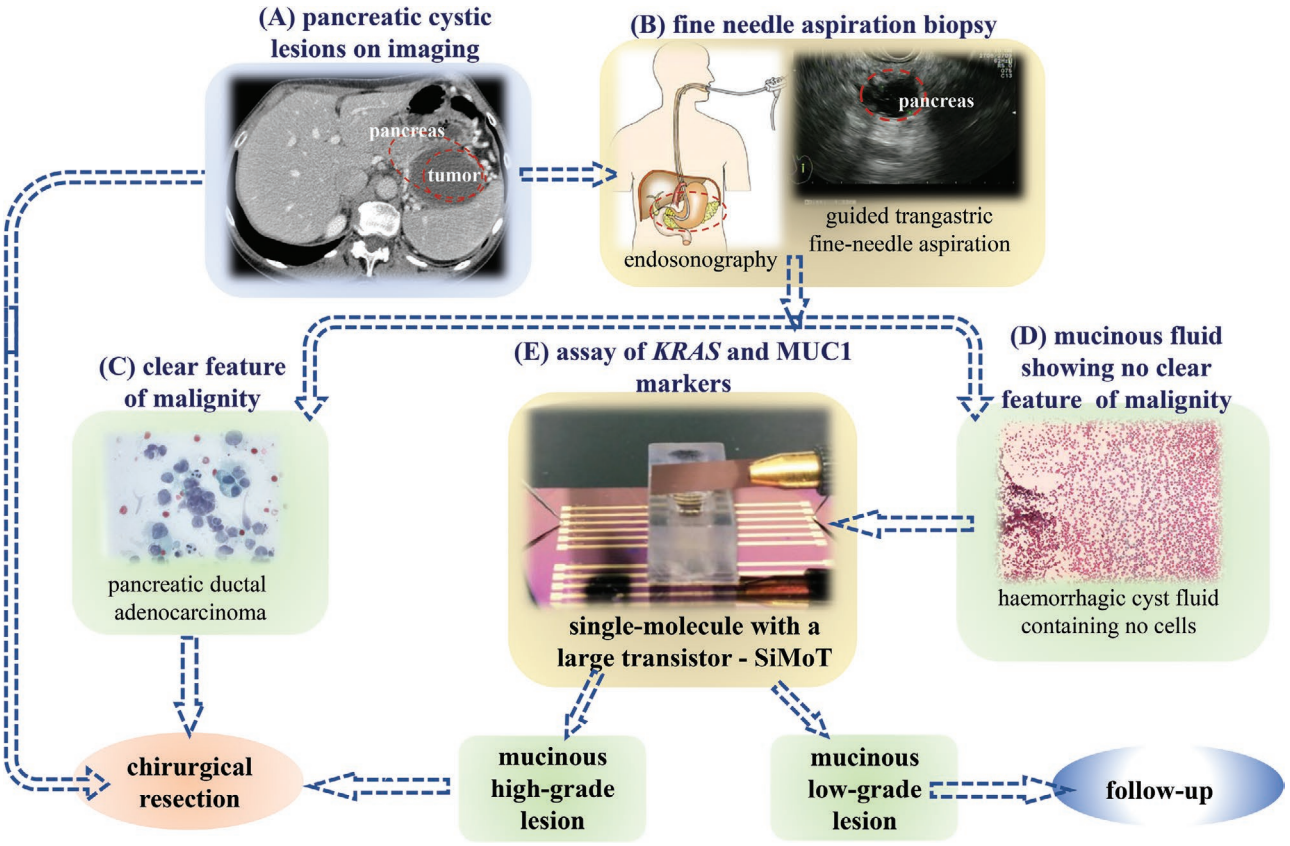

Figure 1. Main steps in current approach to the diagnosis of a neoplastic pancreatic cyst. The steps that can be undertaken to manage a timely diagnosis of a high-grade mucinous lesion likely to evolve into a pancreatic cancer are schematically illustrated. (A) was reproduced from the Medical Clinic for Gastroenterology, Infectiology and Rheumatology.

Studies based on imaging techniques indicate a prevalence of 49% of pancreatic cysts with a diameter larger than 2 mm in asymptomatic individuals.[6] So, a tens of millions of people worldwide have a pancreatic cyst and do not know it. Neoplastic pancreatic cysts make up to 10–15% of all the cysts and about 60% of them are mucinous cysts, namely intraductal papillary mucinous neoplasms and mucinous cystic neoplasms, both precursors of pancreatic ductal adenocarcinoma. Hence, the correct and timely diagnosis of mucinous pancreatic cysts, especially those with high risk of progression, is of utmost importance.

In **Figure 1** the main steps in the foreseen approach to the diagnosis of a neoplastic pancreatic cyst are illustrated. The process starts with the clinical evaluation and the acquisition of cross-sectional images, such as for instance by computer tomography. If clear imaging signs of malignancy are detected (Figure 1A), the indication for surgery is set. When a cystic lesion is identified, the further diagnostic steps are decided according to the recently published *European guidelines on pancreatic cystic neoplasms*.[7] Generally, endosonography with transgastric or transduodenal fine-needle aspiration is carried out to inspect the cyst and collect its fluids (Figure 1B). If malignant cells are detected at cytology, such as in the case of pancreatic ductal adenocarcinoma (Figure 1C), again the indication for surgical resection is set. However, the sensitivity of the fine-needle aspiration cytology for the diagnosis of mucinous pancreatic cystic lesions is quite low being about 50–60%. This is mostly due to the fact that in about 40% of the cases, the sampled material contains no cells to inspect or only degenerated cells (Figure 1D) that are inadequate for diagnosis.[8] The diagnostic sensitivity, that is, the fraction of true-positives over all the positive-to-the-test,[8] can discriminate low-grade from high-grade mucinous cystic lesions, the latter being more likely to undergo malignant transformation. With a diagnostic sensitivity to discriminate mucinous cysts of only up to 75%, cytopathology is clearly inadequate to sort them out. When the carcinoembryonic antigen assay is carried out conjunctly, diagnostic sensitivity can reach up to a maximum of 83%, which is still not adequate.[8]

Accurate discrimination between low-grade and high-grade mucinous cystic lesions makes the diagnosis faster with an impact on costs and on prognosis. The elicited guidelines[7] provide figures supporting the improvement in the diagnosis accuracy of mucinous cysts when suitable markers are analyzed, possibly at the single-molecule level. To this end, an ultimately performing assay platforms such as next-generation sequencing (NGS),[9] can be essential. NGS is indeed capable to sequence genomic markers at the single-copy level, enabling a mucinous cyst diagnostic sensitivity of 91% and a diagnostic specificity (fraction of true-negatives over all the negatives-to-the-test) of 100%.[10,11] Eventually, NGS analysis of genes frequently mutated in mucinous cysts, such as *KRAS*, *GNAS*, and

TP53 in a cyst fluid, is recommended for cases in which a clear diagnosis would affect management. However, the diagnostic sensitivity in detecting high-grade cysts that should immediately undergo resection, remains relatively low (77%).[12]

A valid approach to improve the diagnostic sensitivity of high-grade mucinous lesions, enabling a quick diagnostic statement, is to tackle several biomarkers simultaneously. Relevantly they should all be detected with the lowest possible limit-of-detection[13] as they are not present in a normal cell population. Hence, the presence of even one single molecule can already evidence the onset of a pathologic state. Cancers arise from genetic mutations and/or epigenetic changes originating, in turn, specific alterations of the proteins expressed in the affected cells. Hence, besides the elicited genomic markers, already detected at the physical limit by NGS, also proteins should be engaged.[14] In pancreatic cysts, the oncoprotein Mucin1 (MUC1) is expressed in cells of high-grade precursors of cancer and often also in pancreatic cancer itself. Indeed, the expression of MUC1 is indicative of an aggressive phenotype related to a high frequency of metastases and a poor prognosis. It can also be detected in the serum, as it can be cleaved from the epithelial cells and released into circulation.[15]

Ultra-sensitive protein detections with a system suitable to work in a clinical environment was extremely challenging until the Single-Molecule-Array (Simoa)[16,17,18] platform was commercialized. Simoa can detect proteins at LODs in the 10^{-18} M range[17] or slightly lower.[19] Since thousands of proteins can be found in a volume of 100 µL of a 10×10^{-18} M solution, the Simoa technology is less sensitive than NGS, which can detect a single-molecule (copy of the genomic marker) in a comparable volume. Moreover, Simoa and NGS are bench-top systems not entirely fit for fast, point-of-care applications. Better suited to this aim are the label-free biosensing technologies for point-of-care.[20] *KRAS* and MUC1 markers have been assayed so far with different biosensing technologies,[21,22,23,24,25] exhibiting LODs in the low femtomolar range for Mucin proteins and at the attomolar for genomic markers. It is a fact that a single platform able to address the assay of both proteins and genomic markers, according to the same standards and level of performance, is lacking.[26,27,28] In this respect a significant advancement is offered by the "Single-Molecule assay with a large Transistor—SiMoT"[29] platform (Figure 1E) which sets an unmet world record in label-free single-molecule detection of both proteins and genomic markers. Indeed, label-free single-molecule detection of proteins,[30,31,32,33] peptides[34] and DNA markers[35] have been demonstrated even in serum. Other groups have independently proven the effect, too.[36,37] Moreover, because the platform is label-free, it is also rapid with a time-to-response of some minutes.

In the present work, *KRAS* and MUC1 mucinous lesions markers' have been successfully assayed in phosphate buffer solution (PBS) and whole human blood serum at the physical limit with the same platform, namely the elicited SiMoT one. This represents a compelling proof of principle that can enable a better diagnostic-sensitivity of high-grade mucinous lesions. Moreover, the extremely low detection limits also in whole human blood serum, open to the possibility of performing a diagnosis based solely on the assay of the markers in a peripheral fluid, which would be of great relevance to complement the much more invasive biopsy procedures currently performed.

2. Results

2.1. The "Single-Molecule Assay with a Large Transistor—SiMoT" Device Structure

The sensing measurements were carried out with the SiMoT device whose main features are schematized in **Figure 2**. It comprises a millimeter-sized transistor that integrates a layer with 10^{11}–10^{12} biological recognition elements. The device structure (Figure 2A) is based on an electrolyte gated organic field-effect transistor (EGOFET) fabricated on a plastic foil,[38] comprising an ink-jet printed poly(3-hexylthiophene)—P3HT organic semiconductor as channel material, contacted via interdigitated source (S) and drain (D) electrodes (Figure 2B). Importantly, the organic bioelectronic device herein proposed is fabricated with large-area compatible cost-effective procedures. The main peculiarity of an EGOFET consists in engaging an electronic insulating and ionic conducting electrolyte (even deionized water),[39] serving as the dielectric that couples the transistor channel with the gate electrode. A comprehensive description of the EGOFET operational mechanisms is provided elsewhere,[27,38] and it is hence beyond the scope of the present manuscript. Here we just recall that a source-drain current modulation is triggered by gating the semiconducting channel via the high capacitances ion-modulated electrical-double-layers (EDLs) installed at the gate/electrolyte and electrolyte/P3HT interfaces.

The SiMoT device is further endowed with two gates both immersed, along with the EGOFET channel, in the water (HPLC-grade) electrolyte. A coplanar *lateral gate* (Figure 2A,B) conveniently serves as reference electrode enabling a constant check of the device current level and hence of the device stability. The details and the mechanism of the printed P3HT stabilization have been extensively studied and reported elsewhere.[40,41] In Figure 2B a micrograph of the source and drain interdigitated electrodes and of the circular lateral gate are shown. As anticipated, the electrodes are patterned by photolithography on a plastic foil and the channel area of the interdigitated electrodes is covered with an inkjet-printed P3HT film, in a combination of highly parallelazible and cost-effective processes. The second gate, addressed as the *sensing gate*, is millimeter sized and is made of a gold thin-film (50 nm) deposited by thermal evaporation through a shadow mask on a poly(ethylene 2,6-naphthalate) substrate (Figure 2C). This surface is biofunctionalized with the markers' recognition elements. The sensing gate hangs over the channel at a fixed distance from the EGOFET channel, so that it can be removed from the measuring electrolyte for incubation in the solutions to be assayed.

2.2. The Gate Functionalization Protocol

The core of the SiMoT device is the biofunctionalized self-assembled monolayer (SAM) attached to the gold surface of

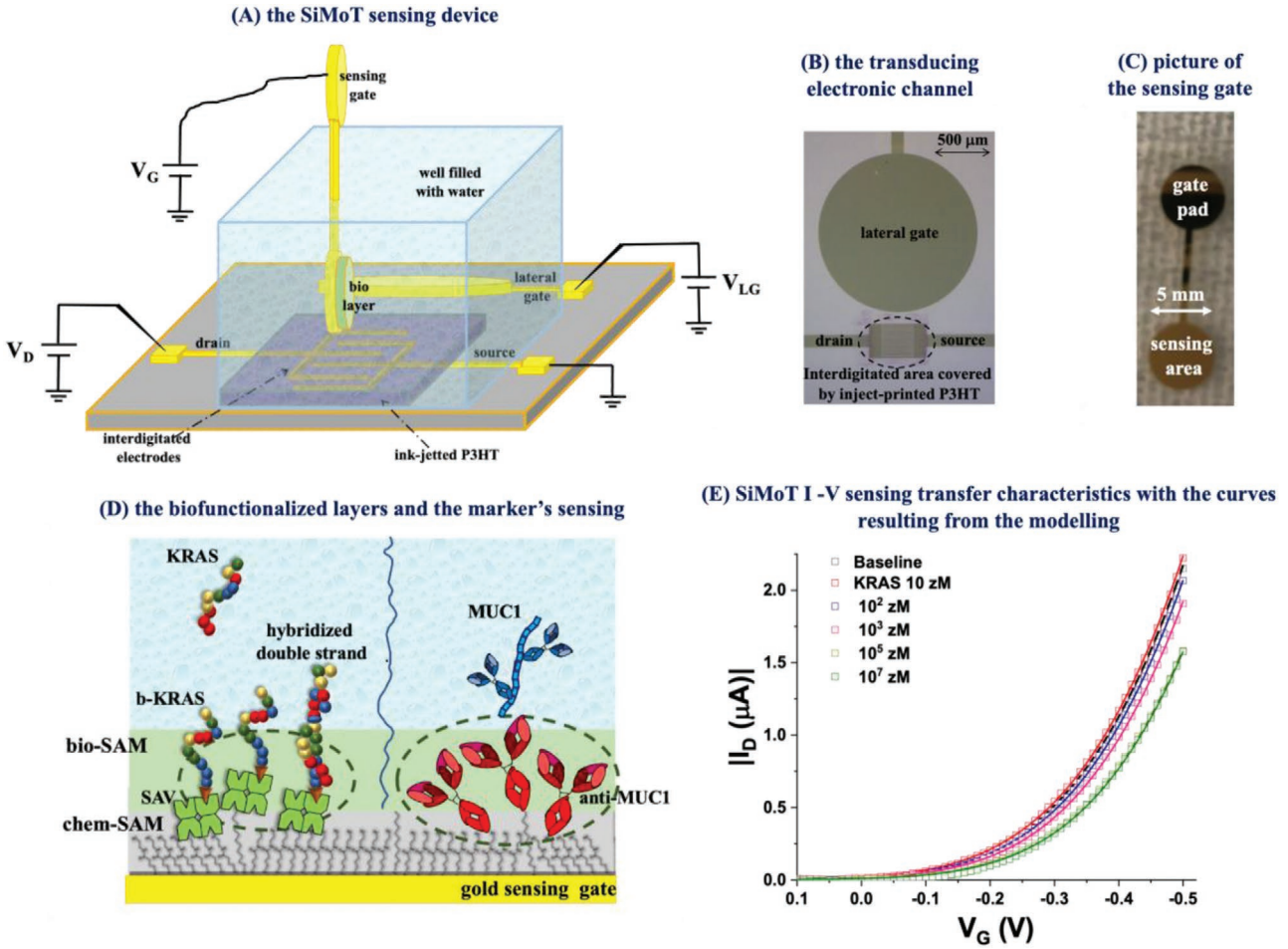

Figure 2. The SiMoT device structure and the single-molecule sensing measurements. A) A schematic of the "Single Molecule assay with a large Transistor—SiMoT" device structure; B) a micrograph of the transistor channel with its interdigitated source and drain electrodes covered by inkjet-printed P3HT along with the coplanar gold lateral gate; C) picture of the sensing gate; D) a pictorial view of the anti-MUC1 and b-*KRAS* bio-SAM layers grafted on the chem-SAM; E) the SiMoT sensing transfer characteristics (I_D vs V_G at $V_D = -0.3$ V). The black-curve correspond to the b-*KRAS* functionalized gate incubated in the sole PBS solution. The same gate is further exposed, in sequence, to PBS standard-solutions of *KRAS* at concentrations of: 10×10^{-21} M (red-curve), 100×10^{-21} M (blue-curve), 1×10^{-18} M (magenta-curve), 100×10^{-18} M (dark-yellow-curve), and 10×10^{-15} M (dark-green-curve). The hollow squares are the experimental data, while the solid lines are the result of the modeling (see text for details).

the sensing gate. The main features of the biofunctionalization protocols,[29,35] are the given in the following. The SAMs of recognition elements serve to bind the marker of interest, selectively. For the experiments carried out in this work, two sensing gates were used: one functionalized with the anti-MUC1, serving as capturing protein for the MUC1 marker, and the other functionalized with the b-*KRAS* a biotinylated DNA single-strand complementary to the gene sequence of *KRAS*. The layers of biological recognition elements, addressed as the bio-SAMs, are covalently attached to a chemical SAM (chem-SAM) of mixed alkanethiols namely: 3-mercaptopropionic acid—3MPA and 11-mercaptoundecanoic acid—11MUA. The rationale for the choice of a mixed SAM to maximize the density of grafted proteins is extensively discussed elsewhere.[42,43] The terminating carboxylic functionalities are, then, activated with ethyl-3-(3-dimethylaminopropyl)-carbodiimide (EDC) and *N*-hydroxysulfosuccinimide sodium (sulfo-NHS). Afterward, the anti-MUC1 antibodies are covalently attached to the chem-SAM enabling the selective MUC1 assay. To saturate the unreacted sulfo-NHS activated groups, the SAM was further treated with ethanolamine. To minimize non-specific binding, the biofunctionalized gate was immersed in a bovine serum albumin (BSA) phosphate buffer saline (PBS) solution.

Conversely, for the *KRAS* sensing, streptavidin was covalently attached to the chem-SAM with the same strategy adopted to attach the antibodies. Afterward, a biotinylated single strand complementary to *KRAS* (b-*KRAS*) was attached to the gate surface, exploiting the strong biotin-streptavidin binding. This adds generality to the SiMoT biofunctionalization process as virtually any biotinylated recognition element can be bound to the gate surface. Indeed, the same strategy was adopted to bind biotinylated peptides serving to recognize peptides markers with a complementary aminoacidic sequence.[34] The anti-MUC1 and b-*KRAS* biofunctionalization strategies are sketched in Figure 2D.

The Surface Plasmon Resonance (SPR) characterization of the anti-MUC1 and b-*KRAS* capturing layers was carried out and the SPR traces at the different steps of the biofunctionalization process are given in Figure S1 in the Supporting Information. The surface coverage of the sensing gate, resulting from the biofunctionalization process, was estimated to be: 7.42×10^{11} molecules cm^{-2} for anti-MUC1 and 4.01×10^{11} molecules cm^{-2} for b-*KRAS* (see Section S1 in the Supporting Information for details). This considerable high number of recognition elements endows the SiMoT transistor with selectivity and enables the occurrence of amplifying cooperative effects that make the single-molecule detection possible with a large transducing interface (vide infra).[29]

2.3. The Single-Molecule Sensing Protocol

The sensing measurements were performed with the SiMoT platform by measuring the transistor current-voltage curves as the source-drain current (I_D) versus the gate bias (V_G) at a fixed source-drain bias (V_D) with a semiconductor parameter analyzer equipped with a probe station, in air, in darkness and at RT (20–22 °C). Before proceeding with the sensing measurements, the device was stabilized by simple immersion in deionized HPLC-grade water for about 24 h. Afterward, I_D was further stabilized by cycling the measurement of the transfer curve via the gating of the EGOFET channel with the lateral reference gate. The duty cycle involved measuring a transfer curve every half an hour until the current drift was reduced to less than 1% h^{-1}, as reported elsewhere.[40] It was demonstrated that this procedure can be carried out once for all, after the deposition of the P3HT film, provided the device is always kept under water after the stabilization is accomplished. Further on, it was proven that a suitable packaging of the device, foreseeing, for instance, a hydrogel mat put in contact with the channel, can keep the device always in a water environment and hence stable for several weeks.[41] Hence the stabilization of the semiconductor does not add to the time-to-results.

The sensing measurements were performed, afterward, according to the following protocol. Each sensing gate, for either the protein or the genomic assay, was washed thoroughly with HPLC water, and mounted inside the EGOFET cell filled with deionized water serving as the electrolyte. A set of 20 transfer characteristics, each one measured with a delay of 30 s, was registered by sweeping V_G from 0.1 to –0.5 V. The sensing gate was then removed from the measuring cell and transferred into the sample to be assayed; in the first set of experiments this was a 100 µL of phosphate buffer saline solution (PBS) that reproduced physiological pH and ionic strength. The sensing gate was incubated (at RT and in the dark) in this solution for 10 min. The biofunctionalized gate was then removed from the PBS solution, washed thoroughly with HPLC deionized water, placed back into the EGOFET cell, and a new set of transfer characteristics was registered until the stabilization was reached. After the measurement of a stable baseline, the sensing biofunctionalized gate was immersed and incubated for 10 min in 100 µL of the PBS standard-solutions containing the MUC1 or the *KRAS* marker at concentrations ranging from 0.1×10^{-21} to 10×10^{-15} M. After incubation in each of the PBS standard-solutions, the sensing gate was washed thoroughly with HPLC-water to remove the unreacted ligands and a further set of I_D–V_G transfer curves were measured. During each incubation step, the lateral coplanar gate current was also monitored continuously registering five transfer characteristics, each with a delay of 30 s in the same voltage window used to bias the sensing gate. This ensured that the current level was not changing by more than a 3–5% percent during the whole set of sensing measurements. The measured final and stable I_D–V_G curves at each concentration for the *KRAS* sensing in PBS are given in Figure 2E as square symbols. Due to the needed stabilization, the I_D–V_G curves measurement at each concentration takes about 30 min. With a single device the measurements at each concentration are performed sequentially. Future development of the SiMoT technology into an array will parallelize the process so that the overall time will be 30 min or less as further optimizations are foreseen.

Physical-based modeling of the I_D–V_G transfer curves for all the sensing measurements was undertaken to extract threshold voltage (V_T) shift at each concentration.[28,44,45] This is a much more robust and reproducible parameter than the current value at a given gate bias. To this end, the electrical measurements were fitted with a numerical model that considers both the charge transport in the P3HT semiconductor and the ion-modulated EDLs accumulation at the electrolyte-semiconductor and at the gate-electrolyte interfaces. All the details of the modeling are provided in the Section S2 in the Supporting Information. By virtue of an example, the I_D–V_G characteristics predicted by the model for the *KRAS* sensing in PBS are shown in Figure 2E as solid lines and the geometrical and physical model parameters are listed in Table S1 in the Supporting Information. As it is apparent, the accordance with the measured data is exceptionally good. Relevantly, the geometrical parameters are measured, the P3HT electronic parameters are taken from the literature or provided by first-principles pseudo-potential density functional calculations, while the P3HT density of localized states, the EDL capacitance per unit area at the electrolyte/P3HT interface, and the threshold voltage (V_T) are calculated from the measured electrical characteristics before performing the bioelectronic sensing.

Then, we accurately reproduced all the sensing characteristics as a function of the analyte concentration by varying only V_T while keeping the same set of all the geometrical and physical model parameters. The accuracy of the physical-based model demonstrates that the sensing measurements of both the MUC1 and *KRAS* markers, as well as the corresponding control experiments, rely on a change in the EGOFET work function that is directly mirrored in a shift of V_T.[29] Negative control experiments were carried out by performing ad hoc designed experiments. In the protein assay negative control dose-curves involved detecting MUC1 against a sensing gate biofunctionalized with a non-binding protein such as BSA. For the genomic assay, negative control dose curves involved detecting a genetic sequence identical to that of *KRAS* except for one single mismatch in the 14th base. This was assayed against the same b-*KRAS* probe giving a non-binding response.

Notably, the detections of MUC1 and *KRAS* and the elicited negative control experiments were also performed in whole human blood serum. In this case, the biofunctionalized

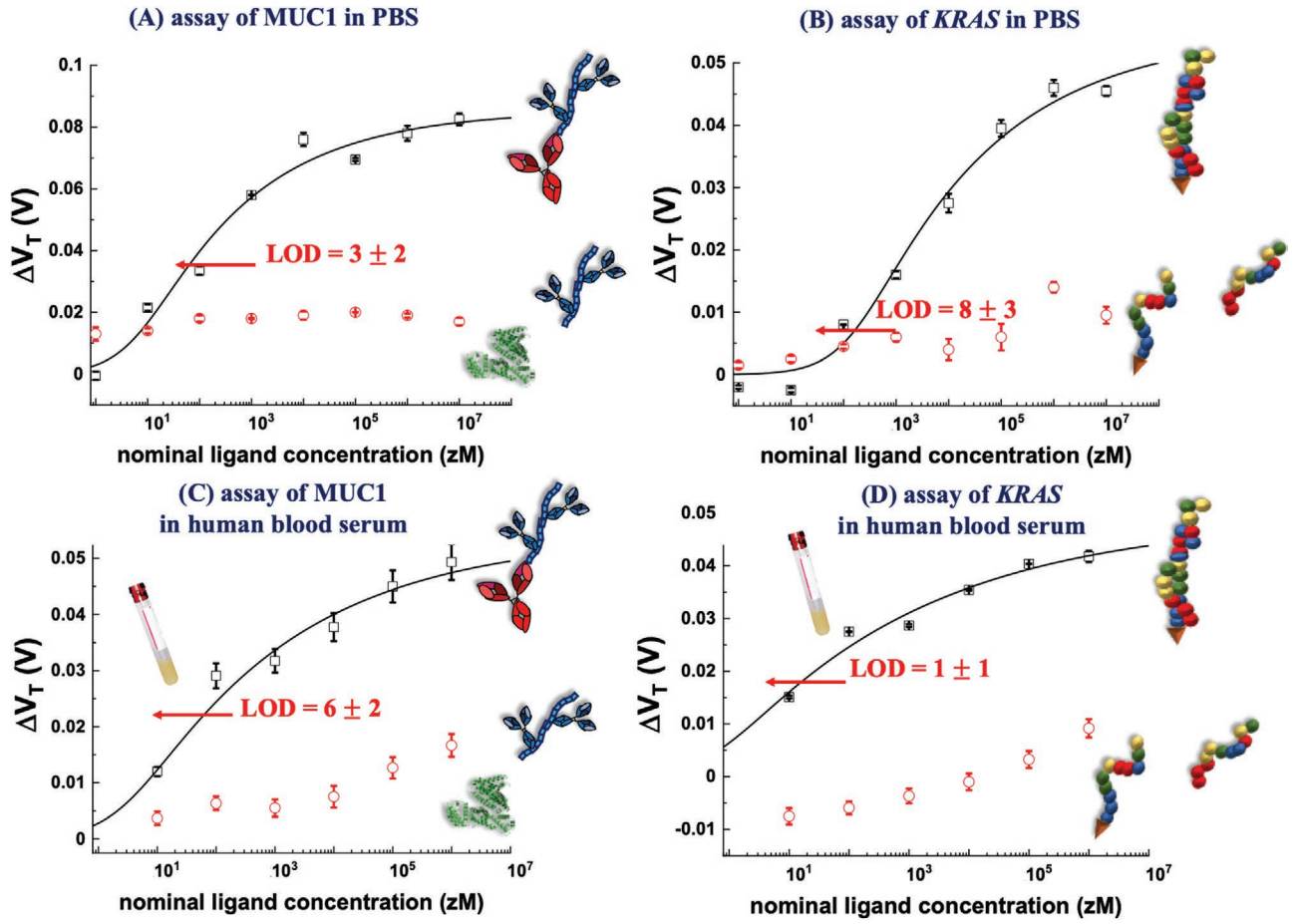

Figure 3. The MUC1 and *KRAS* single-molecule assays in PBS and whole blood serum. A) MUC1/anti-MUC1 affinity binding calibration-curve (hallow black-squares) are shown as the shift of the V_T voltage (ΔV) versus the MUC1 concentration. A BSA biofunctionalized gate serves in the control experiment (hallow red squares). B) *KRAS*/b-*KRAS* affinity binding calibration-curve (hallow black-squares) are shown as the shift of the V_T voltage (ΔV) versus the *KRAS* concentration. A *KRAS* with one mismatch serves in the control experiment (hallow red squares). C,D) The same experiments of panels (A) and (B) are performed in whole human serum. All the data points are given as the average of at least three replicates and the solid lines are the results of a modeling (see text for details).

sensing gates were incubated for 10 min in 100 µL of whole human serum spiked with standard-aliquots of the markers in PBS solution. The maximum volume of PBS added to the whole human serum was 0.2%. The resulting nominal concentrations of MUC1 and *KRAS* in the human blood serum also ranged from 10×10^{-21} to 1×10^{-15} M.

2.4. The MUC1 and *KRAS* Single-Molecule Assays in PBS and Whole Blood Serum

In **Figure 3** the threshold voltage shifts evaluated using the physical-based modeling of the measured I_D currents for the genomic and the protein assay, carried out both in BSA and in whole human serum are given. The full lines, also given in Figure 3, result from the SiMoT dose-curve modeling (vide infra),[29,30,35] which enabled to estimate the LODs accurately. The analytical function that models the dose-curves, measured with the SiMoT, is based on the assumption that the probability for a certain number of cognate ligands to interact with binding sites follows a Poisson distribution (vide infra).[30] Therefore, the LODs were calculated as the concentration responding (ΔV_T shift upon sensing) equal to the average of the noise level of the negative control data in the whole concentration range plus three times the noise' standard-deviation.[13] The computed LOD concentrations [LOD] are: for MUC1 in PBS the LOD level is at 34 mV, resulting in a [LOD] of 50×10^{-21} M; for *KRAS* in PBS the LOD level is at 18 mV, resulting in a [LOD] of 48×10^{-21} M; for MUC1 in whole human serum the LOD level is at 24 mV, giving a [LOD] of 117×10^{-21} M; for *KRAS* in whole human serum the LOD level is at 18 mV, giving a [LOD] of 13×10^{-21} M.

By computing the number of molecules as [LOD] · V · N_A, with V being 100 µL and N_A being the Avogadro's number, the following holds: for MUC1 in PBS a LOD of 3 ± 2 molecules is evaluated; for *KRAS* in PBS a LOD of 8 ± 3 molecules results; for MUC1 in whole human serum the LOD is of 6 ± 2 molecules; -for *KRAS* in whole human serum the LOD is of 1 ± 1 molecules. The Poisson sampling errors in the LODs are customarily computed as the square root of the number of particles. As it is apparent all the SiMoT assays performed, even

those in whole blood serum, detect at the physical limit both proteins and genomic markers.

3. Discussion

Label-free single-molecule detection methods generally proposed so far involve nanometric interfaces that bear the capturing elements, e.g. antibodies to bind an antigen marker or DNA strands to bind a marker with a complementary genomic sequence.[26] Due to the limited interfacial area available on a nanometric transducer, only a few recognition elements can be hosted. Relevantly, the size compatibility between the single marker to be detected and the biofunctionalized transducing interface assures a sufficiently high signal-to-noise-ratio. There is, however, a drawback: in the design of a label-free assay involving a nanometric transducer, one must consider that the few capturing elements on the nanometric transducer and the single marker to be detected are necessarily dispersed in a large volume of at least 10–100 µL. Under these circumstances, the probability that the marker, diffusing following the Stokes-Einstein law, interacts with the nanometric-detecting interface and binds to the recognition element is extremely low, making the experiment unsuitably long. In fact, under the assumption that a micrometer cube volume of 1 fl is the maximum space that a marker can span to interact with its recognition element on the minute time-scale,[18] the concentration of the marker to be assayed is to be in the nanomolar range or higher. At this concentration, the volume to be assayed has a marker in each femtoliter. Hence, wherever the nanometric interface ends up in the sampled volume, there will always be a marker sufficiently close by, to collide with the transducing interface, eventually binding to one of the few recognition elements. A signal is then generated at the nanometric transducer that is sufficiently high to be detected. This proves that the concentration of a sample that can be assayed with a nanometric interface is at least in the nanomolar range, hence 10–11 orders of magnitude far from the tens of zeptomolar that is the concentration of the fluid to be assayed if one wants to detect a single molecule in 100 µL. This is indeed the scope of an assay designed for the early detection of a clinically relevant marker. Eventually, it becomes clear that the label-free single-molecule detections with single nanopores,[46] nano-transistors[47] and other similar approaches, are inherently unable to sense a marker in a large milieu. Or more specifically, to assay a solution that has a concentration in the tenths of zeptomolar, and hence nanometric transducing interfaces cannot be engaged as ultra-sensitive assays for clinical applications.[26]

To enable the assay of a fluid from a patient containing an extremely low concentration of a given marker, an effective approach is to increase the number of recognition-elements by a large amount. Indeed, if a number, e.g. 10^{11}, of transducing interfaces are available in 100 µL, instead of a single nanodevice, wherever the marker is, there will be an interface close enough to detect it. This detecting strategy has been achieved by an operation principle, addressed as *wide-field capturing*, which is effective but generally label-based.[48] Conversely, the electronic detections using field-effect transistor systems with large detecting interfaces are very interesting.[49,50,51] They are generally characterized by being label-free and small, e.g., handheld, hence convenient for use in diagnostics and monitoring in hospital emergency rooms and limited resource settings. Attractive characteristics as compared to central laboratory testing are also: lower volume samples and reagents consumed, small form factors, rapid turn-around times offering, in some cases, also self-testing to patients without requiring hospital visits. In this respect, EGOFETs based on electronic-channel materials such as graphene,[52,53] poly(3,4-ethylenedioxythiophene) polystyrene sulfonate (PEDOT-PSS)[54] and poly(3-hexylthiophene-2,5-diyl) (P3HT),[26,27,29,30,31] have been successfully engaged as wide-field organic bioelectronic sensors exhibiting limit-of-detections at zeptomolar–attomolar level also in real biofluids. Interestingly, electronic driven point-of-care systems also offer the unique and very relevant advantage to enable the sharing of the data immediately with healthcare providers through the read-out system and wireless connectivity. Indeed, self-testing and immediate electronic data-transmissions can result in extremely important time and resources savings. Recently, a graphene based EGOFET has been proposed as bioelectronic-sensor of odors,[53] achieving a LOD as low as 40×10^{-18} M and a rapid response-time of less than 1s. Lately, the SiMoT was proposed as a label-free system endowed with an all-electronic transducing system and data transmission technology that can detect with single-molecule sensitivity, both protein, and genomic markers. So far, a single device system has been fabricated by printing, and hence it can be prospectively produced by large-area and cost-effective procedures. The data collected are also in principle available right away for transmission via fast connections. The experiments shown in Figure 3 clearly prove that SiMoT can detect *KRAS* and MUC1 markers at the physical limit both in PBS and human serum. Remarkably, the experiments reported in Figure 3 have been performed measuring 24 different gates that served in sensing and control experiments and involved the use of 4 different ink-jet printed organic electronic devices, showing an unprecedented reproducibility error within 3% at most. It is worth mentioning that each of those 24 gates, after recording a stable *baseline*, has been subsequently exposed to 8 different standard-solutions of biomarkers at concentrations ranging from 0.1×10^{-21} to 10×10^{-15} M. Moreover, half of the sampled gates have been assayed in real human blood serum spiked with standard-aliquots of the analytes. The control experiments need to be improved in the latter fluid as some features suggest a non-negligible effect of non-specific binding. The plan is to design a control experiment performed with the gate biofunctionalized with the recognition element that assays a healthy patient. Nonetheless, still also under these non-ideal circumstances, LODs are the lowest ever reported with a label-free technology amenable for clinical diagnostics.

Importantly, the physical based modeling of the SiMoT I_D versus V_G curves upon exposure to increasing nominal ligand concentrations foresees that, along with the channel current, only the threshold voltage, V_T, is affected by the binding events (see Section S2 in the Supporting Information). This is expected as the gate is designed to be about two orders of magnitude larger than the EGOFET channel area and the SAM is a high capacitance, ion-permeable membrane very responsive to electrostatic changes.[29] Remarkably, the variation of V_T provides a direct quantitative information about the variation of

the biofunctionalized electrode work-function upon biorecognition events. More in detail, the bio recognition event(s) trigger a local variation of the SAM dipole orientation that propagates through the hydrogen-bonding network and eventually results in a variation of the surface energy (*viz*. work-function) of the biofunctionalized electrode.[29,30] In addition, it is worth mentioning that V_T is calculated by accurately modelling the full I_D–V_G characteristic measured at various concentrations, thus ensuring a robust and reliable information, which is independent of possible fluctuation of the drain current at one fixed gate voltage. Relevantly, the physical based model, reported in Section S2 in the Supporting Information, has been validated on more than 4000 electrical characteristics, being therefore extremely accurate and reliable.

The core of the SiMoT technology is the already introduced electrolyte-gated FET endowed with a millimeter-wide gate that is biofunctionalized with 10^{12} recognition elements capable to detect selectively down to one single marker in 100 µL. This means being able to assay a sample at a concentration of a few tens of zeptomolar. The very large transducing interface, when immersed in 100 µL, makes it highly probable for few markers to reach by diffusion the gate surface in the time frame of 10 min.[55] So, although counterintuitive, wide-field sampling can also be achieved by engaging a sufficiently large capturing interface, populated by trillions of recognition elements. Once the binding occurs, the single-molecule event involves one recognition element, and detecting this event is like spotting the wave generated by a single droplet of water falling on the surface of a one-kilometer-squared wide pool. Under these circumstances, the critical issue is to understand how the signal-to-noise ratio can be sufficiently high to measure a significant signal. In Simoa, the amplification effect is associated with the catalytic activity of the enzyme. In NGS, there is a combined effect of the polymerase chain reaction amplification and the pH-sensitive FET transduction. The SiMoT takes advantage of the EGOFET amplification effects contributing roughly with a factor of 10^3,[27] which is, however, not enough to make a single binding event signal significantly high when trillions of other recognition elements populate the same transducing interface. So, a second amplification phenomenon is to be considered, which has not been fully deciphered yet. However, a model involving molecular dynamic simulations has been developed[29,30]. It foresees that amplification occurs, associated with a hydrogen-bonding network that connects the chains of the chem-SAM and likely involves the bio-SAM, too. This system enables a collective effect that amplifies the single binding event. When the binding occurs, while it involves just one recognition element, it generates a defect in the network of hydrogen bonding that, in the presence of the electric field associated with the gate bias, has a certain degree of order. The defect generated in the network propagates eventually fueled by the gating field itself.[27] A shift of the gate work function involving a large number of recognition elements populating an area much larger than the one occupied by the two interacting species, eventually supposedly occurs.

Along this line, also the modeling of the sensing dose curves, based on the Poisson distribution probability of single binding events, was performed.[29] The result of the modeling is provided as solid lines in the four panels of Figure 3. The model envisages that the SAM is divided into domains constituted by a certain number of recognition elements. The domains are limited by electrostatic active defects populating their boundaries. If one marker binds to any of the recognition elements in one domain, this binding event is modelled to trigger a shift of the work function involving the whole domain, by the propagation of the effect that is limited by the defective boundary. As anticipated, this is foreseen as possible due to collaborative interactions propagating the work function change due to a rearrangement (dipole change) in the recognition elements that populate the domain around the binding. Eventually, an irreversible and stable shift of the work function, within that domain is generated, which then returns a signal significantly larger than the noise.

4. Conclusion

In conclusion, the electronic detection-based technology presented herein provides a feasible perspective to improve the diagnostic sensitivity for the detection of high-grade mucinous pancreatic cysts by detecting both genomic and protein markers with the same ultimate sensitivity. Indeed, we could demonstrate that *KRAS* and MUC1 markers are detected in phosphate buffer saline solution as well as in whole blood serum with single-molecule detection limits. Prospectively, the SiMoT technology will be developed into an all-electronic array that will perform multiplexing of several markers directly into a peripheral biological fluid, such as blood. This will possibly open to an extremely important use of liquid biopsy for the diagnosis of pancreatic cancer precursors thus integrating and improving current diagnostic procedures. The proposed approach is also general and opens unexplored opportunities for early diagnostic and personalized medicine.

5. Experimental Section

Materials: Poly(3-hexylthiophene)—P3HT (regioregularity > 99%) with an average molecular weight (M_W) of 20 000–45 000 g mol^{-1}, was purchased from Sigma-Aldrich. The organic semiconductor was used with no further purification. Poly(ethylene 2,6-naphthalate) (PEN) substrate, with thickness 125 µm, has been purchased from Du Pont. 3-mercaptopropionic acid (3-MPA), 11-mercaptoundecanoic acid (11-MUA), 1-ethyl-3-(3-dimethylaminopropyl)-carbodiimide (EDC), *N*-hydroxysulfosuccinimide sodium salt (sulfo-NHS) were purchased from Sigma-Aldrich and used with no further purification. Mucin 1 monoclonal antibody (anti-MUC1) with M_W = 25.1 kDa purified from mouse ascites fluids or tissue culture supernatant by affinity chromatography, and recombinant protein of human mucin 1 (MUC1), M_W 25.1 kDa, was purchased from Origene and used with no further purification. Streptavidin (SAV) from Streptomyces avidinii lyophilized from 10 × 10^{-3} M potassium phosphate was purchased from Sigma-Aldrich and used with no further purification. *KRAS* oligonucleotides was purchased from Invitrogen-Thermo fisher Scientific and readily used. Biotinylated-*KRAS* G12D fwd (sequence: 5′-TGCCTACGCCATCAGCTCCAACTAC), M_W 7914 Da, was used as biorecognition element; this is addressed as b-*KRAS* in the text. The *KRAS* G12D rev (sequence: GTAGTTGGAGCTGATGGCGTAGGCA), M_W 7835 Da, was used as target oligonucleotides. This is addressed as *KRAS* in the text. The negative control experiments were performed using

KRAS G12D 1MM (sequence: GTAGTTGGAGCTGGTGGCGTAGGCA) as analyte with 1 mismatch in base 14th and M_W 7835 Da. Water (HPLC-grade, Sigma-Aldrich) and ethanol grade puriss. p.a. assay, ≥ 99.8%, were used with no further purification. Phosphate buffered saline (PBS, Sigma-Aldrich) solution presents osmolality and ion concentrations matching those of the human body (isotonic). One tablet of PBS was dissolved in 200 mL of water (HPLC-grade), resulting into 0.01 M phosphate buffer, 0.0027 M potassium chloride, and 0.137 M sodium chloride, pH 7.4, at 25 °C. Human serum produced from fresh whole blood of a healthy donor aged between 18 and 60, screened and tested negative for HIV, Hepatitis B and C, has been purchased from Research Donors Ltd., London (UK).

Electrolyte Gated Organic Thin-Film Transistor Fabrication: Printed EGOFETs were fabricated on a PEN plastic substrate. Gold source (S), drain (D) and circular lateral gate (LG) electrodes, were patterned by a lift-off photolithography procedure based on a reverse flood exposure process. This process was adapted, optimized and applied on circular, 6 inches PEN substrates, making it suitable also for the fabrication of large arrays of sensors. With this technique, a single photoresist layer was required (AZ5214E, MicroChem). It was first spin coated on the substrate (1 min at 4000 r.p.m.), then baked at 110 °C for 90 s in order to remove the solvent and then subjected to a negative exposition using a mask aligner (Karl Süss MA6/BA8) and negative photolithographic mask (custom made by CompuGraphics). The crosslinking of the exposed parts of the resist was then carried on by baking at 120 °C for 90 s. The following flood exposure of the whole sample allows to obtain the desired pattern after development in AZ 726 MIF developer. Before the thermal evaporation of gold (30 nm), an adhesion layer of chromium (2 nm) was deposited over the PEN substrate. The lift-off step was carried out overnight by immersion of the sample in TechniStrip Microdeposit D2 stripper. Finally, the samples were cleaned in a ultrasonic bath in both acetone and IPA, dried with nitrogen and further cleaned by means of oxygen plasma for 2 min. The obtained geometrical dimensions are as follows: channel width of 10 500 µm; channel length of 5 µm; circular lateral gate diameter of 2.5 mm. The P3HT was dissolved in a blend of chlorobenzene (CB) and ortho-dichlorobenzene (ODCB), in a ratio of 75/25, at a concentration of 2.6 mg mL^{-1} and then inkjet printed by means of a Fujifilm Dimatix DMP-2831 only over the channel area through a cartridge with 10 pL nozzles. The ink was printed at a drop spacing of 45 µm (one layer), a firing voltage of 40 V, a jetting frequency of 1 kHz, with the plate temperature set to 35 °C. Finally, in order to reduce the leakage current, a film of a biocompatible insulator (SU8-TF6001 MicroChem) was inkjet printed on top of the gold traces, excluding the channel and the lateral gate areas. The device was treated with and annealing at 130 °C for 8 h in a nitrogen environment. Then, a polystyrene (PS) cell of ≈2 cm^3 was glued on the substrate around the channel area with PDMS. The cell was filled with ≈2 mL of water (HPLC-grade, Honeywell Riedel-de Haën) serving as the gating medium. The sensing gate, made of thermally evaporated gold 50 nm thick on PEN foil, has a diameter of 5 mm and the track has been passivated with Scotch 3M Magic tape. The gate has been stably positioned inside the cell filled with water in correspondence of the electrodes interdigitated area. Details on the printed EGOFETs fabrication and characterization have been reported elsewhere.[41]

Gate Biofunctionalization Protocol: The gate electrodes were cleaned by means of sonication in 2-propanol for 10 min and subsequently rinsed with HPLC water, dried with N_2 and then treated for 10 min in ozone cleaner. The gate biofunctionalization protocol, described in details elsewhere,[42] involves as first step the immobilization of a chemical SAM (chem-SAM) on the gold surface comprising a 10×10^{-3} M solution of 3-MPA to 11-MUA (10:1 molar ratio) in ethanol. The cleaned gold surface was dipped inside the 3-MPA and 11-MUA solution and kept in the dark under constant N_2 flux for 18 h at 22 °C. The resulting monolayer will be addressed in the following as the chemical SAM (chem-SAM). The strong gold-sulfur interaction results in the exposure of the carboxylic groups, activated subsequently by reacting the gate electrode in a 200×10^{-3} M 1-Ethyl-3-(3-dimethylaminopropyl) carbodiimide (EDC) and 50×10^{-3} M sulfo-*N*-Hydroxysuccinimide (sulfo-NHS) aqueous solution for two hours at 25 °C. The biofunctionalization protocol then proceeds according to the following steps for the i) protein and ii) and genomic biorecognition element immobilization. (i) The anti-MUC1 antibody was then conjugated to the activated COOH sites reacting with the terminal amine groups of the antibody. To this end, the gate has been immersed in an anti-MUC1 PBS solution for 2 h at 25 °C. The solution comprises 4×10^{-3} M (0.1 mg mL^{-1}) of anti-MUC1 and PBS at a pH of 7.4 and an ionic-strength (i_s) of 162×10^{-3} M. The unreacted sulpho-NHS groups were saturated, afterward, with ethanolamine (1 M in PBS 10×10^{-3} M) for 1 h at 25 °C. Finally, the biofunctionalized gate was immersed in a 1.5×10^{-6} M (0.1 mg mL^{-1}) BSA solution in PBS 10×10^{-3} M for 1 h at 25 °C. This was meant to minimize non-specific binding. For the control experiment of MUC1 biomarker a gate was biofunctionalized with BSA (0.1 mg mL^{-1}) according to the same protocol. (ii) In the case of genomic biological recognition elements, the gate surface with activated carboxylic groups was immersed in a SAV phosphate buffer saline (PBS) solution for 2 h at 25 °C. The solution comprises 1.5 µM (0.1 mg mL^{-1}) of SAV in PBS at pH 7.4. Afterward, the SAV SAM was further treated with ethanolamine 1 M in PBS 10×10^{-3} M for 1 h at 25 °C. Finally, the gate was immersed in a biotinylated *KRAS* (0.5 µM) PBS solution at pH 7.4 for 2 h at 25 °C. Eventually, for both protocols (i) and (ii) after each step of the biofunctionalization, the gate was washed with the corresponding solvent to remove possible unbounded residues. In the text, the following notation has been adopted, namely SAM is relevant to the layer comprising both the chem-SAM and the bio-SAM.

Supporting Information

Supporting Information is available from the Wiley Online Library or from the author.

Acknowledgements

Prof. Eugenio Cantatore, Dr. Piero Larizza, Dr. Guillaume Fichet, and Prof. Gaetano Scamarcio are acknowledged for useful discussions. SiMBiT—Single molecule bioelectronic smart system array for clinical testing (Grant Agreement ID: 824946), PMGB -Sviluppo di piattaforme meccatroniche, genomiche e bioinformatiche per l'oncologia di precisione—ARS01_01195—PON "RICERCA E INNOVAZIONE" 2014–2020, Academy of Finland projects #316881, #316883 "Spatiotemporal control of Cell Functions,", #332106 "ProSiT—Protein Detection at the Single-Molecule Limit with a Self-powered Organic Transistor for HIV early diagnosis," Åbo Akademi University CoE "Bioelectronic activation of cell functions" and CSGI are acknowledged for partial financial support.

Conflict of Interest

The authors declare no conflict of interest.

Author Contributions

E.M. developed the biofunctionalization process and performed the sensing measurements; L.S. and A.T. also worked at the biofunctionalization procedure and performed the SPR characterization of the gates; C.D. contributed to the definition of the clinical aspects of the markers' assay; Z.G., A.T., and R. Ö. fabricated the sensing gate and contributed to the device electrical characterization; G.P. did the modeling of the dose curves; F.T. and Z.M.K.V. designed the devices and performed the modeling of the transfer characteristics; F.V. and

F.M. fabricated the printed EGOFETs under the supervision of M.C. L.T coordinated the whole effort, the part of the SiMoT system development and the assays, i.e., for the medical/clinical aspects. L.T. wrote the first draft of the manuscript and all the authors contributed to revise it.

Data Availability Statement

The data that support the findings of this study are available on request from the corresponding author. The data are not publicly available due to privacy or ethical restrictions.

Keywords

electrolyte-gated field-effect-transistors, organic bioelectronic sensors, pancreatic cancer, pancreatic cysts, single-molecule assay

Received: March 24, 2021
Revised: June 1, 2021
Published online: June 19, 2021

[1] GBD 2017 Pancreatic Cancer Collaborators, *Lancet* **2019**, *4*, 934.
[2] J. Ferlay, E. Steliarova-Foucher, J. Lortet-Tieulent, S. Rosso, J. W. W. Coebergh, H. Comber, D. Forman, F. Bray, *Eur. J. Cancer* **2013**, *49*, 1374.
[3] Eurostat, https://appsso.eurostat.ec.europa.eu/nui/show.do?dataset=hlth_cd_asdr2&lang=en (accessed: May 2021).
[4] P. Rawla, T. Sunkara, V. Gaduputi, *World J. Oncol.* **2019**, *10*, 10.
[5] A. Vincent, J. Herman, R. Schulick, R. H. Hruban, M. Goggins, *Lancet* **2011**, *378*, 607.
[6] E. Crowley, F. Di Nicolantonio, F. Loupakis, A. Bardelli, *Nat. Rev. Clin. Oncol.* **2013**, *10*, 472.
[7] The European Study Group on Cystic Tumours of the Pancreas, *Gut* **2018**, *67*, 789.
[8] O. M. Soyer, B. Baran, A. C. Ormeci, D. Sahin, S. Gokturk, S. Evirgen, R. Basar, P. Firat, F. Akyuz, K. Demir, F. Besisik, S. Kaymakoglu, C. Karaca, *Medicine* **2017**, *96*, 5513.
[9] J. M. Rothberg, W. Hinz, J. Bustillo, *Nature* **2011**, *475*, 348.
[10] S. Ngamruengphong, M. I. Canto, *Surg. Clin. North Am.* **2016**, *96*, 1223.
[11] C. Verbeke, L. Haberle, D. Lenggenhager, I. Esposito, *Pancreatology* **2018**, *25*, S1424.
[12] L. Haeberle, M. Schramm, W. Goering, L. Frohn, C. Driescher, W. Hartwig, H. K. Preissinger-Heinzel, T. Beyna, H. Neuhaus, K. Fuchs, V. Keitel-Anselmino, W. T. Knoefel, I. Esposito, *Sci. Rep.* **2021**, *11*, 2901.
[13] M. Thompson, S. L. R. Ellison, R. Wood, *Pure Appl. Chem.* **2002**, *74*, 835.
[14] F. Dinter, M. Burdukiewicz, P. Schierack, W. Lehmann, J. Nestler, G. Dame, S. Rödiger, *Anal. Bioanal. Chem.* **2019**, *411*, 7725.
[15] J. M. Curry, K. J. Thompson, S. G. Rao, D. M. Besmer, A. M. Murphy, V. Z. Grdzelishvili, W. A. Ahrens, I. H. McKillop, D. Sindram, D. A. Iannitti, J. B. Martinie, P. Mukherjee, *J. Surg. Oncol.* **2013**, *107*, 713.
[16] X. Wang, L. Cohen, J. Wang, D. R. Walt, *J. Am. Chem. Soc.* **2018**, *140*, 18132.
[17] S. K. Fischer, A. Joyce, M. Spengler, T.-Y. Yang, Y. Zhuang, M. Scheel Fjording, M. Alvydas, *AAPS J.* **2015**, *17*, 93.
[18] D. M. Rissin, D. R. Walt, *Nano Lett.* **2006**, *6*, 520.
[19] D. M. Rissin, C. W. Kan, T. G. Campbell, S. C. Howes, D. R. Fournier, L. Song, T. Piech, P. P. Patel, L. Chang, A. J. Rivnak, E. P. Ferrell, J. D. Randall, G. K. Provuncher, D. R. Walt, D. C. Duffy, *Nat. Biotechnol.* **2010**, *28*, 595.
[20] S. Shrivastava, T. Quang Trung, N.-E. Lee, *Chem. Soc. Rev.* **2020**, *49*, 1812.
[21] A. B. Beyenea, B. J. Hwangb, W. A. Tegegnea, J.-S. Wangd, H.-C. Tsaia, W.-N. Sua, *Microchem. J.* **2020**, *158*, 105099.
[22] C.-J. Yang, H. Yan, N. Tang, Y. Zou, Y. Al-Hadeethi, X. Xu, H. Dalir, R. T. Chen, *Micromachines* **2020**, *11*, 282.
[23] Y. Pang, C. Wang, L. C. Lu, C. Wang, Z. Sun, R. Xiao, *Biosens. Bioelectron.* **2019**, *130*, 204.
[24] D. Zeng, Z. Wang, Z. Meng, P. Wang, L. San, W. Wang, A. Aldalbahi, L. Li, J. Shen, X. Mi, *ACS Appl. Mater. Interfaces* **2017**, *9*, 24118.
[25] M. Pan, J. Cai, S. Li, L. Xu, W. Ma, C. Xu, H. Kuang, *Anal. Chem.* **2021**, *93*, 4825.
[26] E. Macchia, K. Manoli, C. Di Franco, G. Scamarcio, L. Torsi, *Anal. Bioanal. Chem.* **2020**, *412*, 5005.
[27] E. Macchia, R. A. Picca, K. Manoli, C. Di Franco, D. Blasi, L. Sarcina, N. Ditaranto, N. Cioffi, R. Österbacka, G. Scamarcio, F. Torricelli, L. Torsi, *Mater. Horiz.* **2020**, *7*, 999.
[28] M. R. Picca, K. Manoli, E. Macchia, L. Sarcina, C. Di Franco, N. Cioffi, D. Blasi, R. Österbacka, F. Torricelli, G. Scamarcio, L. Torsi, *Adv. Funct. Mater.* **2019**, *30*, 1904513.
[29] E. Macchia, M. K, B. Holzer, C. Di Franco, M. Ghittorelli, F. Torricelli, D. Alberga, G. F. Mangiatordi, G. Palazzo, G. Scamarcio, L. Torsi, *Nat. Commun.* **2018**, *9*, 3223.
[30] E. Macchia, A. Tiwari, K. Manoli, B. Holzer, N. Ditaranto, R. A. Picca, N. Cioffi, C. Di Franco, G. Scamarcio, G. Palazzo, L. Torsi, *Chem. Mater.* **2019**, *31*, 6476.
[31] E. Macchia, K. Manoli, B. Holzer, C. Di Franco, R. A. Picca, N. Cioffi, G. Scamarcio, G. Palazzo, L. Torsi, *Anal. Bioanal. Chem.* **2019**, *411*, 4899.
[32] E. Macchia, L. Sarcina, R. A. Picca, K. Manoli, C. Di Franco, G. Scamarcio, L. Torsi, *Anal. Bioanal. Chem.* **2020**, *412*, 811.
[33] S. K. Sailapu, E. Macchia, I. Merino-Jimenez, J. P. Esquivel, L. Sarcina, G. Scamarcio, S. D. Minteer, L. Torsi, N. Sabaté, *Biosens. Bioelectron.* **2020**, *156*, 112103.
[34] E. Macchia, K. Björkström, V. Eskonen, A. Tewari, A. Luukkonen, A. Ghafari, L. Sarcina, K. Manoli, N. Tong-Ochoa, K. Kopra, F. Pettersson, Z. Gounani, L. Torsi, H. Härmä, R. Österbacka, unpublished **2020**.
[35] E. Macchia, R. A. Picca, K. Manoli, C. Di Franco, G. Scamarcio, G. Palazzo, L. Torsi, *ACS Sens.* **2020**, *5*, 1822.
[36] Y. Wu, X. Wang, X. Li, Y. Xiao, Y. Wang, *Chin. Chem. Lett.* **2020**, *31*, 99.
[37] K. Guo, S. Wustoni, A. Koklu, E. Díaz-Galicia, M. Moser, A. Hama, A. A. Alqahtani, A. N. Ahmad, F. S. Alhamlan, M. Shuaib, A. Pain, I. McCulloch, S. T. Arold, R. Grünberg, S. Inal, *Nat. Biomed. Eng.* **2021**, https://doi.org/10.1038/s41551-021-00734-9.
[38] S. H. Kim, K. Hong, W. Xie, K. H. Lee, S. Zhang, T. P. Lodge, C. D. Frisbie, *Adv. Mater.* **2013**, *25*, 1822.
[39] L. Kergoat, L. Herlogsson, D. Braga, B. Piro, M.-C. Pham, X. Crispin, M. Berggren, G. Horowitz, *Adv. Mater.* **2010**, *22*, 2565.
[40] R. A. Picca, K. Manoli, E. Macchia, A. Tricase, C. Di Franco, G. Scamarcio, N. Cioffi, L. Torsi, *Front. Chem.* **2019**, *7*, 667.
[41] D. Blasi, F. Viola, F. Modena, A. Luukkonen, E. Macchia, R. A. Picca, Z. Gounani, A. Tewari, R. Österback, M. Caironi, Z. M. Kovacs Vajna, G. Scamarcio, F. Torricelli, L. Torsi, *J. Mater. Chem. C* **2020**, *8*, 15312.
[42] B. Holzer, K. Manoli, N. Ditaranto, E. Macchia, A. Tiwari, C. Di Franco, G. Scamarcio, L. Torsi, *Adv. Biosyst.* **2017**, *1*, 1700055.
[43] J. W. Lee, S. J. Sim, S. M. Cho, J. Lee, *Biosens. Bioelectron.* **2005**, *20*, 1422.
[44] F. Torricelli, E. Macchia, P. Romele, K. Manoli, C. Di Franco, Z. M. Kovács-Vajna, G. Palazzo, G. Scamarcio, L. Torsi, *Proc. of Int. Conf. on Simulation of Semiconductor Processes and Devices (SISPAD)*, Institute of Electrical and Electronics Engineers, Piscataway, NJ **2019**.

[45] F. Torricelli, E. Macchia, K. Manoli, C. Di Franco, Z. M. Kovács-Vajna, G. Palazzo, G. Scamarcio, L. Torsi, *8th IEEE Int. Workshop on Advances in Sensors and Interfaces*, IEEE **2019**.
[46] S. Sorgenfrei, C.-y. Chiu, R. L. Gonzalez Jr, Y.-J. Yu, P. Kim, C. Nuckolls, K. L. Shepard, *Nat. Nanotechnol.* **2011**, *6*, 126.
[47] R. Wei, V. Gatterdam, R. Wieneke, R. Tampé, U. Rant, *Nat. Nanotechnol.* **2012**, *7*, 257.
[48] J. Gooding, K. Gaus, *Angew. Chem., Int. Ed.* **2016**, *55*, 11354.
[49] S. Casalini, F. Leonardi, T. Crame, F. Biscarini, *Org. Electron.* **2013**, *14*, 156.
[50] M. Y. Mulla, E. Tuccori, M. Magliulo, G. Lattanzi, G. Palazzo, K. Persaud, L. Torsi, *Nat. Commun.* **2015**, *6*, 6010.
[51] K. Manoli, M. Magliulo, M. Y. Mulla, M. Singh, L. Sabbatini, G. Palazzo, L. Torsi, *Angew. Chem., Int. Ed.* **2015**, *54*, 12562.
[52] S. J. Park, O. S. Kwon, S. H. Lee, H. S. Song, T. H. Park, J. Jang, *Nano Lett.* **2012**, *12*, 5082.
[53] G. Seo, G. Lee, M. J. Kim, S. H. Baek, M. Choi, K. B. Ku, C. S. Lee, S. Jun, D. Park, H. G. Kim, S. J. Kim, J. O. Lee, B. T. Kim, E. C. Park, S. I. Kim, *ACS Nano* **2020**, *14*, 5135.
[54] E. Macchia, P. Romele, K. Manoli, M. Ghittorelli, M. Magliulo, Z. M. Kovács-Vajna, F. Torricelli, L. Torsi, *Flexible Printed Electron.* **2018**, *3*, 034002.
[55] E. Macchia, L. De Caro, G. F. Mangiatordi, F. Torricelli, G. Scamarcio, L. Torsi, *Advanced Science* **2021**.